AJNR

Time-Saving 3D MRI Protocols with Millimeter and Submillimeter Isotropic Spatial Resolution for Face and Neck Imaging As Implemented at a Single-Site Major Referral Center

Jeffrey P. Guenette and Lei Qin

AJNR Am J Neuroradiol published online 31 January 2024
http://www.ajnr.org/content/early/2024/01/31/ajnr.A8184

Published January 31, 2024 as 10.3174/ajnr.A8184
Published as a preprint [DATE]

CLINICAL REPORT

HEAD AND NECK IMAGING

Time-Saving 3D MRI Protocols with Millimeter and Submillimeter Isotropic Spatial Resolution for Face and Neck Imaging As Implemented at a Single-Site Major Referral Center

Jeffrey P. Guenette and Lei Qin

ABSTRACT

MRI has become the routine modality for staging nasopharyngeal carcinoma, evaluating for perineural tumor spread, and detecting cartilage invasion in laryngeal carcinoma. However, these protocols traditionally require in the range of 25 to 35 minutes of acquisition time. 3D sequences offer the potential advantage of time savings through the acquisition of one-millimeter or sub-millimeter resolution isotropic data followed by multiplanar reformats that require no further imaging time. We have iteratively optimized vendor product 3D T1-weighted MRI sequences for morphologic face and neck imaging, reducing the average acquisition time of our 3T protocols by 9 minutes, 57 seconds (40.9%) and of our 1.5T protocols by 9 minutes, 5 seconds (37.0%) while simultaneously maintaining or improving spatial resolution. This clinical report describes our experience optimizing and implementing commercially available 3D T1-weighted MRI pulse sequence protocols for clinical face and neck MRI examinations utilizing illustrative cases. We provide protocol details to allow others to replicate our implementations and we outline challenges we faced along with our solutions.

ABBREVIATIONS: ABC = definition; XYZ = definition.

Received month day, year; accepted after revision month day, year.
From the Division of Neuroradiology, Brigham and Women's Hospital & Dana-Farber Cancer Institute (J.P.G.), and Department of Imaging, Dana-Farber Cancer Institute (L.Q.), and Harvard Medical School (J.P.G., L.Q.), Boston, MA, USA.

The authors report no disclosures.

Please address correspondence to Jeffrey P. Guenette, M.D., M.P.H., Division of Neuroradiology, Brigham and Women's Hospital, 75 Francis Street, Boston, MA 02130, USA; jpguenette@bwh.harvard.edu.

INTRODUCTION

MRI pulse sequence development has largely focused on the brain (small body part that can remain motionless), heart (dynamic imaging techniques), and other organ-specific indications. Pulse sequences have not been specifically designed for imaging the intricate structures of the face and neck, where there are also challenges associated with swallowing and breathing motion and acquiring data through the relatively large head to the thin neck to the wide shoulders. Many radiology groups thus use pulse sequences designed for the brain, shifting the scan range to the face and adding slices for the neck. These vendor product 2D T1-weighted and 2D T2-weighted sequences typically have 5 mm slice thickness and 1 mm slice gaps. Cranial nerves, neural foramina, extrinsic tongue muscles, and other small structures are difficult to visualize on these images, restricting the extent to which imaging can impact clinical management decisions. In centers with subspecialized head and neck radiologists and sufficient MRI physicist and/or technologist resources, vendor product protocols are often adapted to generate higher resolution images, typically along the lines of 3 mm slice thickness with no slice gap and with in-plane resolution of 0.5-0.7 mm (often in the range of 0.75 mm^3 rectangular voxels). With these improvements, MRI has become the routine modality for staging nasopharyngeal carcinoma (1,2), evaluating for perineural tumor spread (3), and detecting cartilage invasion in laryngeal carcinoma (4). However, these protocols require in the range of 25 to 35 minutes of acquisition time. Since May 2021, we have intermittently modified, tested, and implemented more rapid face and neck MRI protocols while aiming to maintain or improve overall spatial resolution and soft tissue contrasts.

Given previous successful optimization of 3D steady state, 3D T2-weighted turbo spin echo, and 3D ultrashort echo time sequences for visualization of the cranial nerves (5–8), we iteratively optimized vendor product 3D T1-weighted MRI sequences for morphologic face and neck imaging. To date, we have modified the T1-weighted acquisitions in our General/Trans-spatial, Nasopharynx/Nasal Cavity, Oropharynx/Oral Cavity, and Sinus MRI protocols. Our optimization process was as follows: (1) the MRI physicist co-author adapted a vendor product pulse sequence protocol for one-millimeter or sub-millimeter resolution imaging of the face and neck region of interest by adjusting field of view, matrix, scan volume, TR, TE, flip angle, bandwidth, and acceleration factors by gestalt based on past experience;

Copyright 2024 by American Society of Neuroradiology.

(2) the new sequence protocol was run on a patient in addition to the standard routine protocol at the time; (3) the neuroradiologist co-author reviewed the images and provided the physicist with constructive criticisms on the subjective quality and the process returned to step (1) or the neuroradiologist was satisfied with the quality and the sequence protocol was adopted. Using this process, we have reduced the average acquisition time for (1) the 3T General/Trans-spatial, Nasopharynx/Nasal Cavity, Oropharynx/Oral Cavity, and Sinus MRI protocols from 24 minutes 21 seconds to 14 minutes 24 seconds, yielding a 9 minute 57 second (40.9%) time savings on average (range: 6 minutes 23 seconds to 13 minutes 18 seconds, 27.7% to 55.4% time savings) and for (2) the same 1.5T protocols from 24 minutes 33 seconds to 15 minutes 29 seconds, yielding a 9 minute 5 second (37.0%) time savings on average (range: 5 minutes 3 seconds to 13 minutes 46 seconds, 21.7% to 59.3% time savings). Total acquisition time for our face and neck MRI protocols is now routinely in the 10-minute to 17-minute range on 3T systems (Table 1). We have simultaneously maintained or improved spatial resolution. For example, we have improved overall spatial resolution in our oropharynx protocol by 35%, decreasing voxel volume from 0.75 mm^3 to 0.65 mm^3.

This clinical report describes our experience optimizing and implementing commercially available 3D T1-weighted MRI pulse sequence protocols for clinical face and neck MRI examinations. We provide protocol details to allow others to replicate our implementations and we outline challenges we faced along with our solutions.

Case Series

Case 1: 3D T1-Weighted Gradient Echo, Turbo Spin Echo, and Fat Suppression Techniques

We began by optimizing T1-weighted gradient recall echo images, called volumetric interpolated breath-hold examination (VIBE) on Siemens systems, before T1-weighted turbo spin echo sequences were available across our scanners. The soft tissue contrast on VIBE images was subjectively considered poor by our neuroradiology faculty relative to the 2D and 3D turbo spin echo images, providing less contrast between fat and muscle while blood vessels also had roughly similar intermediate signal intensity. We therefore turned to 3D T1-weighted turbo spin echo sequences as they became available across our fleet. We use the Sampling Perfection with Application optimized Contrasts using different flip angle Evolution (SPACE) product sequence on Siemens scanners and the CUBE product sequence on GE scanners. Our optimization work has been performed with the SPACE sequence on 3T systems, then applied to the CUBE sequence, and then adapted for 1.5T systems. Direct comparisons of T1-weighted VIBE and SPACE images are provided from a 44-year-old female with neck pain in Figure 1.

For post-contrast imaging, the opportunity to acquire both T1-weighted in-phase images and fat suppressed images in the same acquisition is highly appealing. The fat suppression technique described by Dixon in 1984 (9) includes single-sequence acquisition of both in-phase and opposed-phase data, allowing mathematical processing into four contrasts: T1-weighted in-phase, T1-weighted opposed-phase, T1-weighted water, and T1-weighted fat. The implementation of Dixon with 3D spoiled gradient echo sequence on Siemens systems is called VIBE Dixon and on GE systems is called liver acquisition with volume acceleration flex (LAVA-Flex). Anecdotally, we have found the Dixon technique to be more robust than the spectral fat suppression techniques we use in 2D imaging. Direct comparison of the T1-weighted VIBE Dixon fat suppressed images are provided in Figure 1 in conjunction with the T1-weighted pre-contrast images from the same patient.

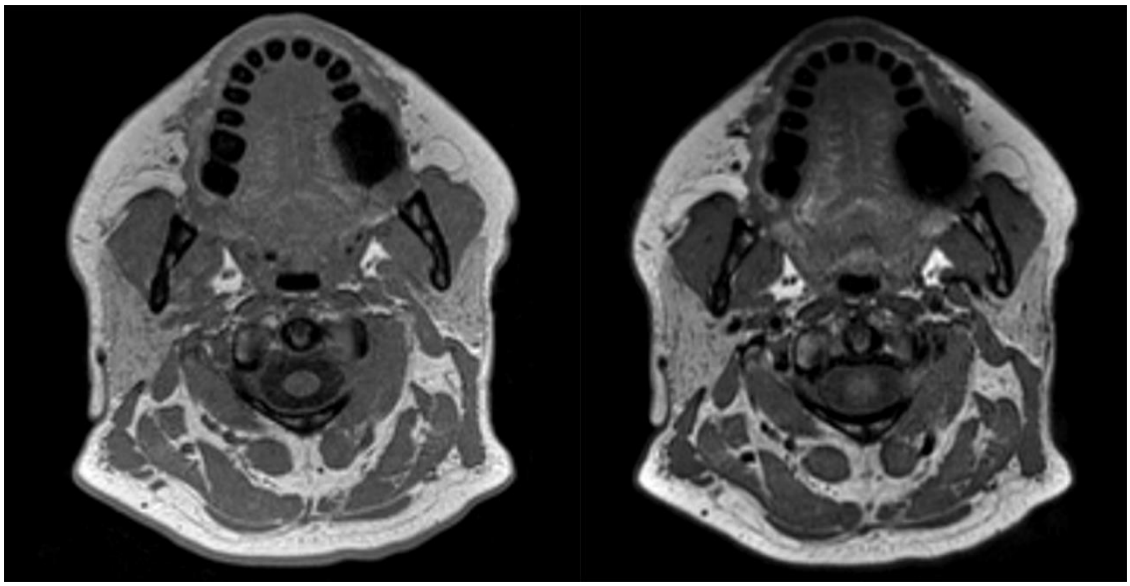

A B

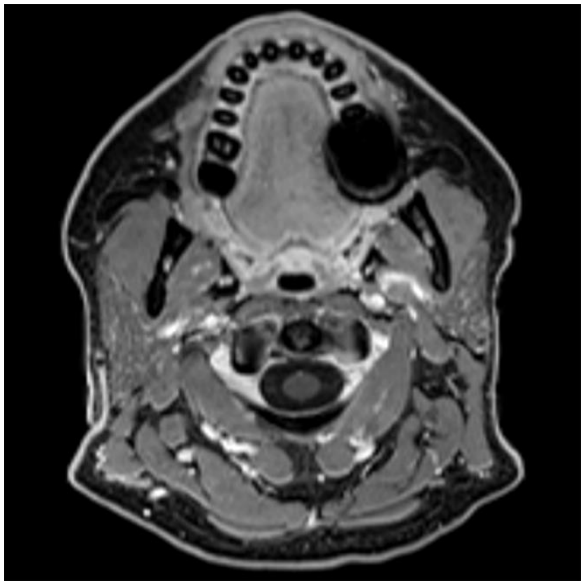

C

FIG 1. Example (A) 3D T1 VIBE, (B) 3D T1 SPACE, and (C) post-contrast 3D T1 VIBE Dixon fat suppression images acquired in the same session on a Siemens 3T Vida system at the level of the oral cavity, retromolar trigone, and parotid glands in a 44-year-old female with neck pain show excellent discrimination of soft tissue structure boundaries with subjectively better soft tissue contrasts on the SPACE than VIBE and robust fat suppression on the VIBE Dixon.

All of our optimized 3D T1-weighted protocol parameters are provided in the Supplemental Material to allow replication at other institutions. Information on our optimized 2D T1-weighted protocols and detailed protocol parameters are provided in the online-only supplemental material.

Case 2: Whole Neck Protocol and Early Protocol Iteration Showing Invasive Cutaneous Lesion

For the non-focal whole neck protocol, we acquire data in the sagittal plane, which minimizes the scan range and eliminates the potential for wrap artifact from the body and vertex scalp. Given that this protocol is used for identification of gross soft tissue abnormalities without necessity for finer spatial detail, we acquire at 1 mm isotropic resolution. However, even at 1 mm3 voxels, this sequence can often more clearly show small lesions than what we traditionally called "high resolution" 2D acquisition images, which were submillimeter in plane but with 3 mm or thicker slice thickness. An example is provided in Figure 2, images from a 92-year-old female with a small focal cutaneous squamous cell carcinoma pre-auricular metastasis invading the parotid gland.

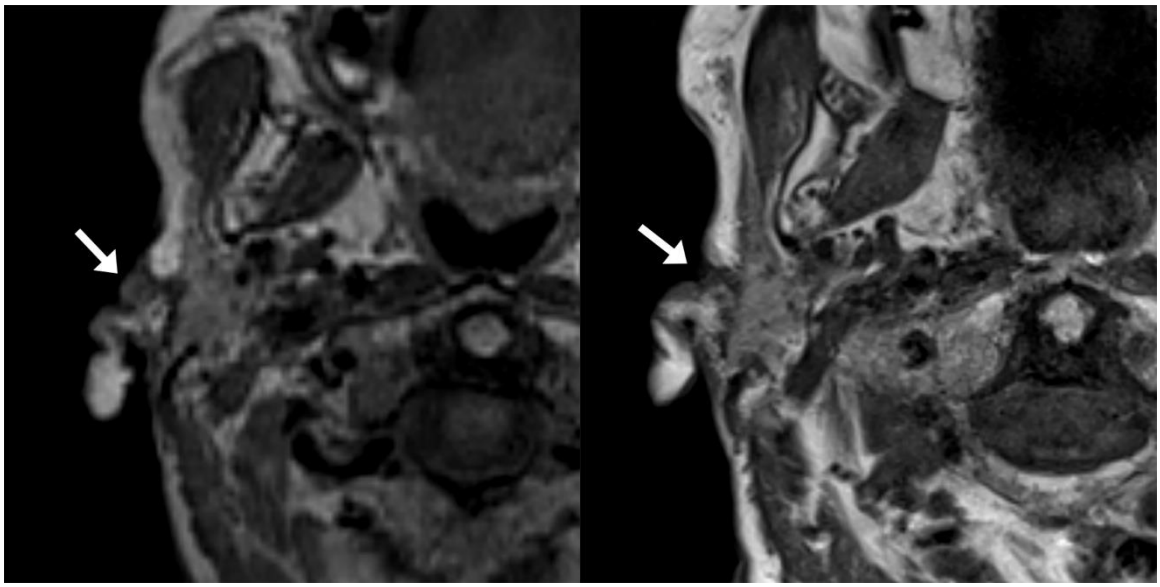

A B

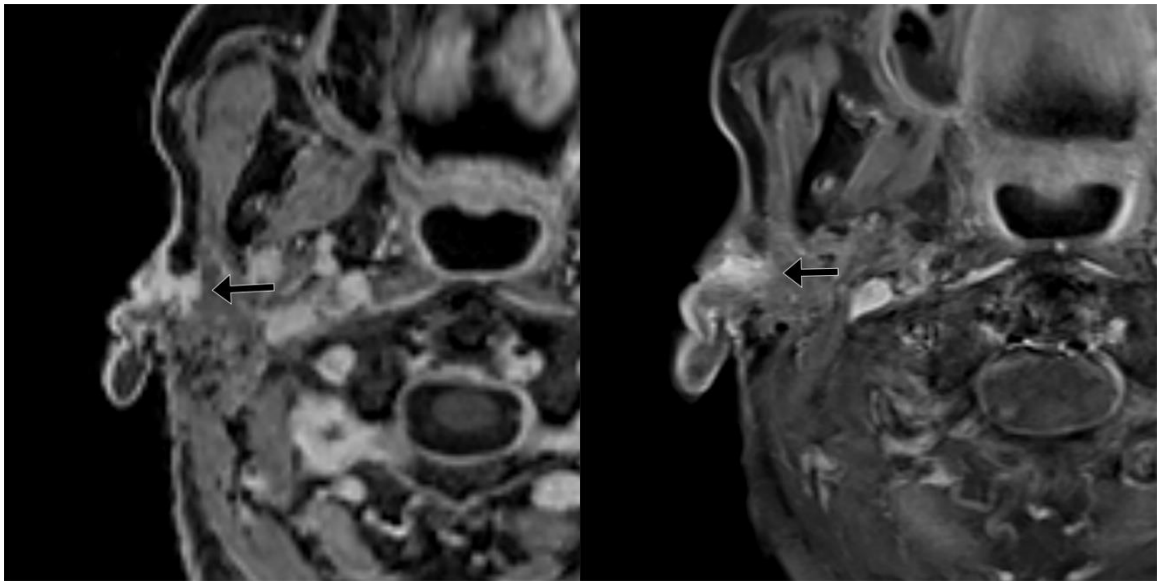

C D

FIG 2. 92-year-old female with squamous cell carcinoma. (A) T1 SPACE performed in the full neck MRI protocol with 2.7mm3 (1.4 mm isotropic) voxels during early optimization iterations reformatted into the axial plane clearly shows a cutaneous preauricular lesion (arrow) that is not visible due to volume averaging on the (B) 2D T1-weighted image with 1mm3 (4x0.5x0.5mm) voxels. The (C) T1 VIBE Dixon reformatting image into the axial plane shows the associated infiltrating tumor into the parotid gland (arrow) to advantage compared with the (D) 2D T1-weighted image with spectral fat suppression. The case encouraged us that the SPACE was a reasonable alternative to the 2D standard-of-care and led us to improve the spatial resolution of the SPACE. These images were obtained contemporaneously on a Siemens 3T Vida system.

Case 3: One-Millimeter Sagittal Isotropic Whole Neck Protocol with 1.5T Adaptation

Our 1.5T protocol was adapted from the 3T protocol to provide the same resolution. 1.5T protocol parameters are provided in the Supplemental Material alongside the 3T protocol parameters. An example is provided in Figure 3, images from a 27-year-old male with right supraclavicular and chest wall desmoid tumor.

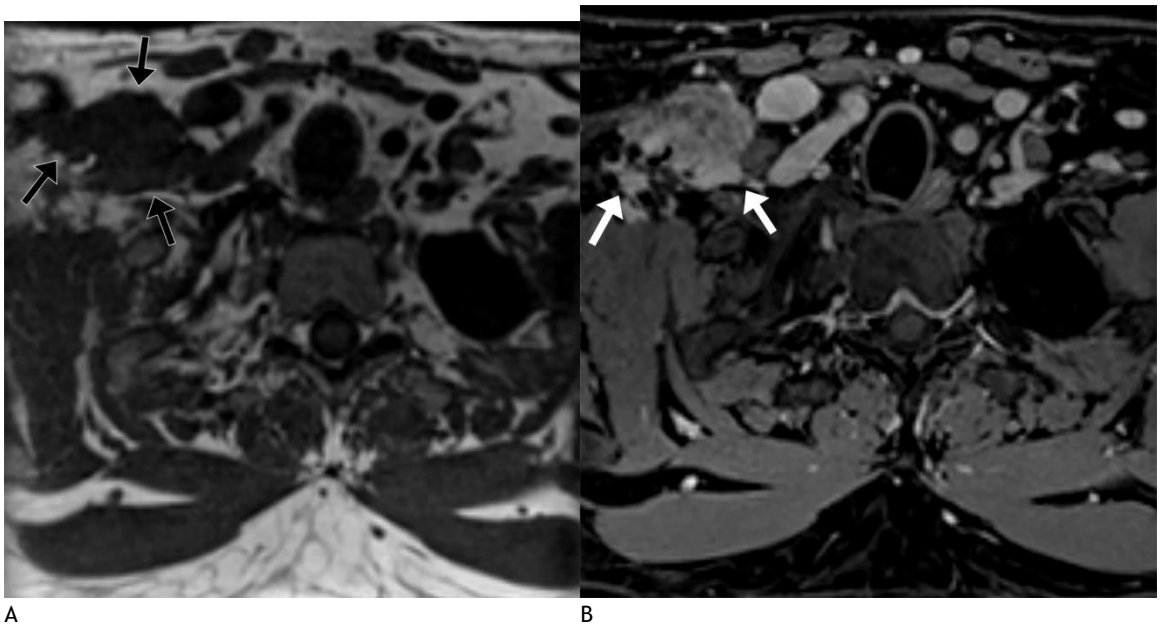

A B

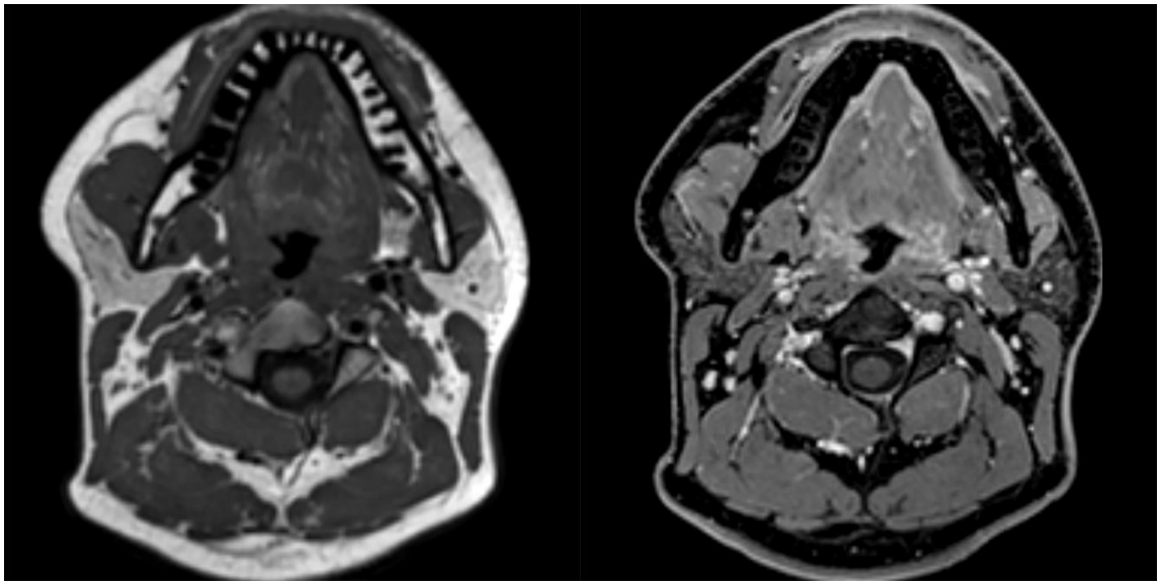

C D

FIG 3. 27-year-old male with right supraclavicular and chest wall desmoid tumor images on a Siemens 1.5T Aera system. The tumor (arrows) is shown on general neck protocol 1.0 mm isotropic sagittal acquisition (A) T1 SPACE axial reformat and (B) T1 VIBE Dixon post-contrast axial reformat images. Image quality and fat suppression remain good at the level of the thoracic inlet. In addition, (C) T1 SPACE axial reformat and (D) T1 VIBE Dixon post-contrast axial reformat images through the face are provided to show image quality in that region.

Case 4: Submillimeter Axial Isotropic Focused Face Protocol

For the higher resolution targeted 3D T1-weighted protocols, we acquire data in the axial plane to minimize the scan range and allow for higher resolution imaging (0.9 x 0.9 x 0.8 mm) in shorter scan times. This approach requires oversampling to avoid wrap artifact. However, even with oversampling and the somewhat longer acquisition time compared with the axial 2D protocol, we achieve considerable time savings due to submillimeter near-isotropic voxels allowing multiplanar reconstructions and elimination of multiple plane acquisitions (Table 1). We minimize axial acquisition time and phase encoding steps by using a left-right phase encoding direction and rectangle field of view (FOV). Reformatting images into the coronal and sagittal planes provides us with 3 planes of T1-weighted imaging through the region of interest. Furthermore, individual radiologists can adjust the isotropic image planes in our PACS viewer to optimize viewing. To give a rough comparison of visual contrast of the 3D images relative to the 2D images of our prior protocol, we measured the signal intensity ratio in 3 consecutive patients who had imaging with the 3D protocol in mid July 2023 and who had prior imaging with the 2D protocol also on a 3T MRI scanner. In this sample, the lateral pterygoid muscle to retroantral fat signal intensity ratio (visual contrast) is similar at 0.41 +/- 0.05 for this 3D protocol compared with 0.35 +/- 0.06 for the 2D protocol.

For post-contrast T1-weighted images, we also acquire data in the axial plane at 0.9 mm isotropic resolution with a left-right phase encoding direction and rectangle FOV to minimize acquisition time. We have compared antero-posterior and left-right phase encoding directions and observed no substantial flow artifact on images using either encoding direction. In the same sample of 3 consecutive patients, retroantral fat to lateral pterygoid muscle signal intensity ratio (visual contrast) is 0.83 +/- 0.07 for this 3D protocol versus 0.38 +/- 0.13 for the 2D protocol for examinations performed at different timepoints; there is greater muscle:fat contrast for the 3D than 2D images.

We show images for this protocol from a 44-year-old female with newly diagnosed oral cavity squamous cell carcinoma in Figure 4.

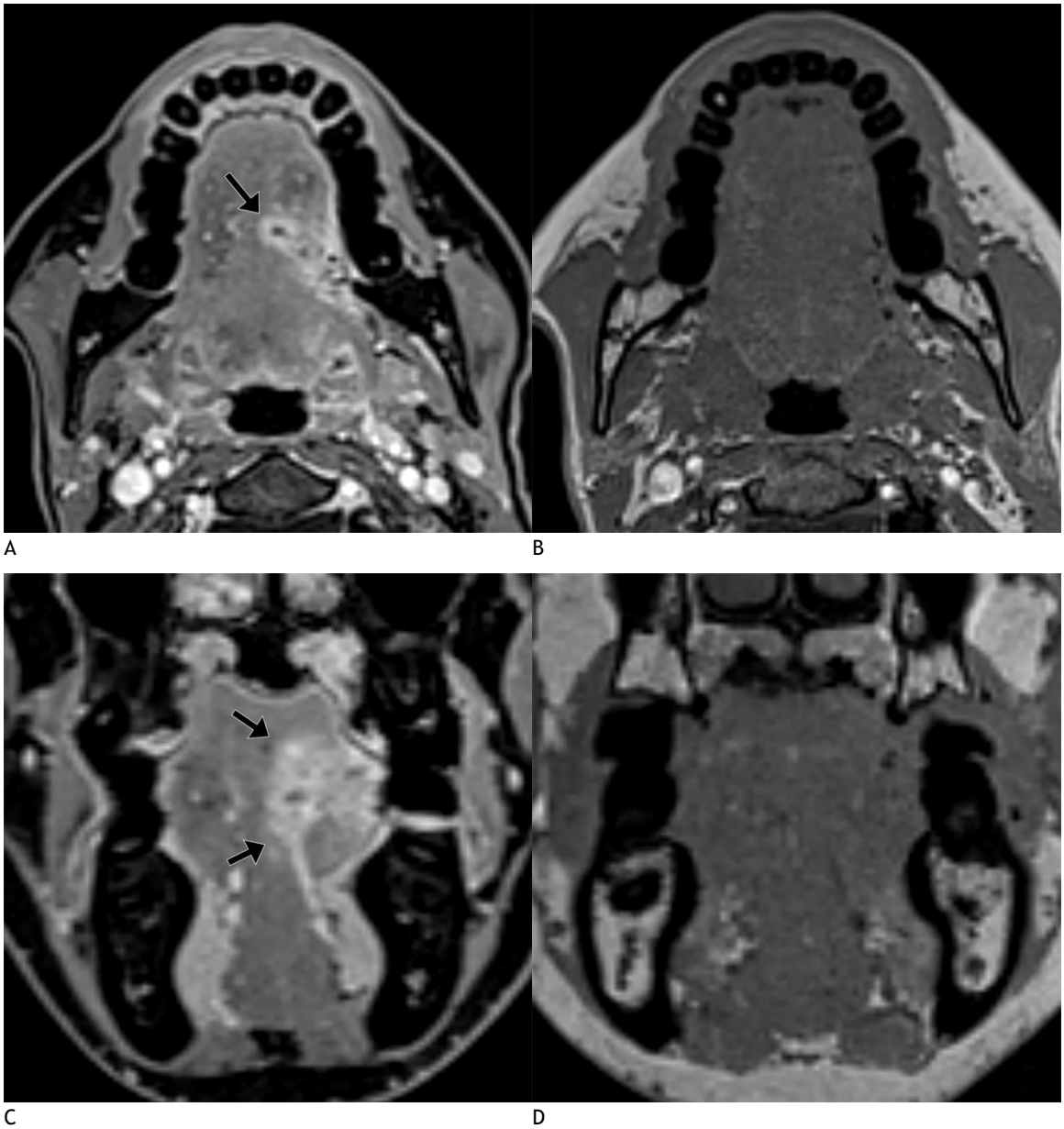

FIG 4. 44-year-old female with newly diagnosed oral cavity squamous cell carcinoma (arrows) shown on oropharynx protocol T1 VIBE Dixon 0.8 x 0.9 x 0.9 mm resolution (A) axial acquisition and (B) coronal reformat images and corresponding pre-contrast T1 SPACE (C) axial acquisition and (D) coronal reformat images obtained on a Siemens 3T Vida system.

Case 5: One-Millimeter Coronal Isotropic Sinus Protocol Showing Nasal Cavity Mass

For sinus imaging we acquire data in the coronal plane, from the tip of the nose to the vertebral bodies, to minimize the scan range and scan times. We show example images of this protocol compared with 2D images for an 83-year-old female with a stable untreated nasal cavity mass of unknown pathology in Figure 5.

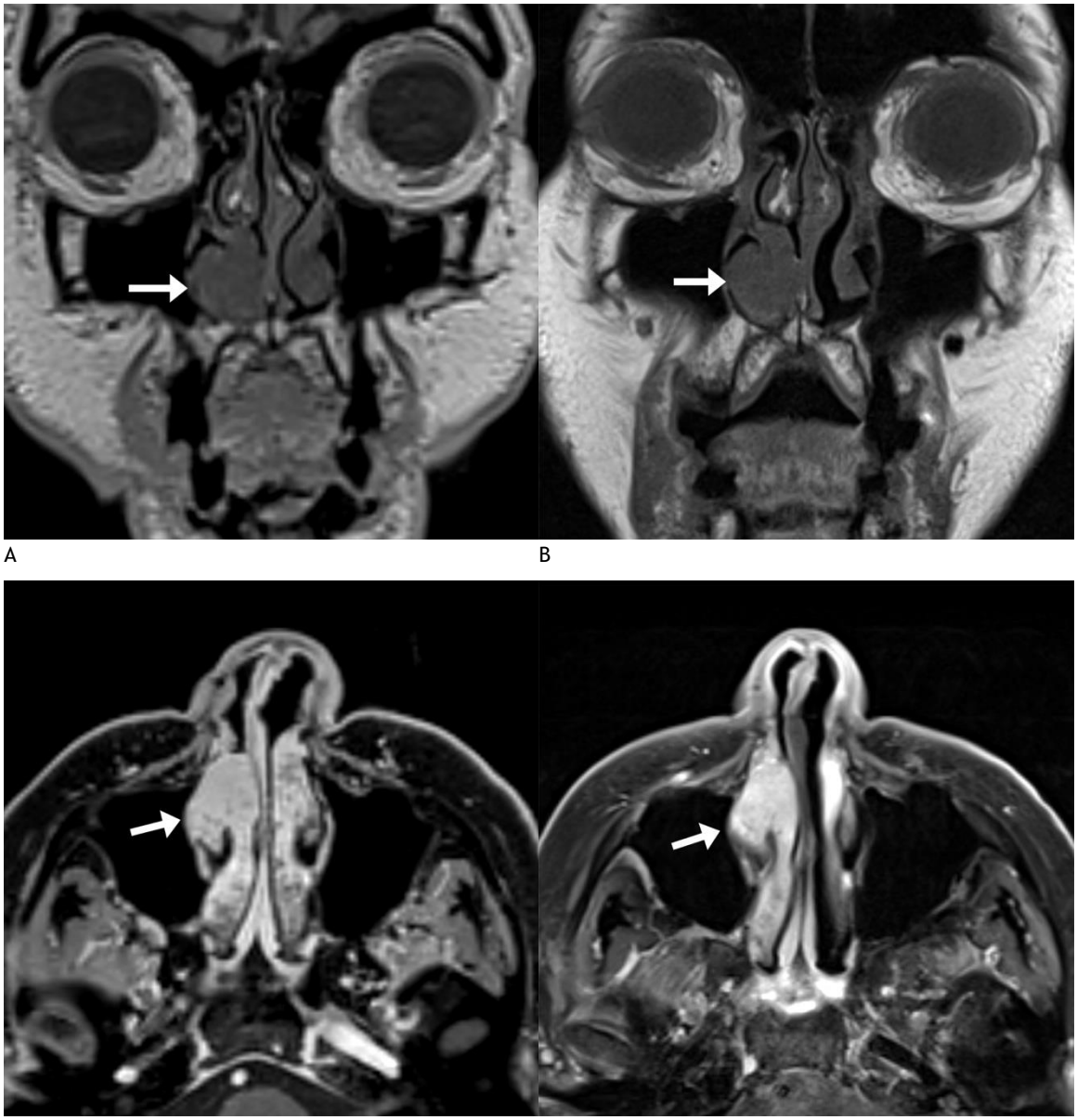

A B

C D

FIG 5. 83-year-old female with melanoma and stable untreated nasal cavity mass of unknown pathology with sinus protocol MRI. (A) T1 SPACE coronal acquisition performed with 1mm3 (1.0 mm isotropic) voxels shows a mass (arrow) along the anterior aspect of the right inferior turbinate, seen similarly on the (B) 2D T1-weighted image with 0.8mm3 (3x0.5x0.52mm) voxels. The (C) T1 VIBE Dixon axial reformat shows the mass (arrow) to advantage compared with the (D) 2D T1-weighted image with spectral fat suppression; the former shows the extent of mass relative to more heterogeneously enhancing turbinate. The 3D images were acquired on a Siemens 3T Vida system 6 months following the acquisition of the 2D images on a 3T Siemens Skyra system.

Case 6: Submillimeter Coronal Isotropic Sinus Protocol Showing Perineural Tumor

During our optimization phase, we tested submillimeter coronal acquisitions in our sinus protocol, similar to our high-resolution axial protocol for nasopharynx and oropharynx. We show an example of perineural tumor from one of these examinations in an 85-year-old male with spindle cell sarcoma in Figure 6.

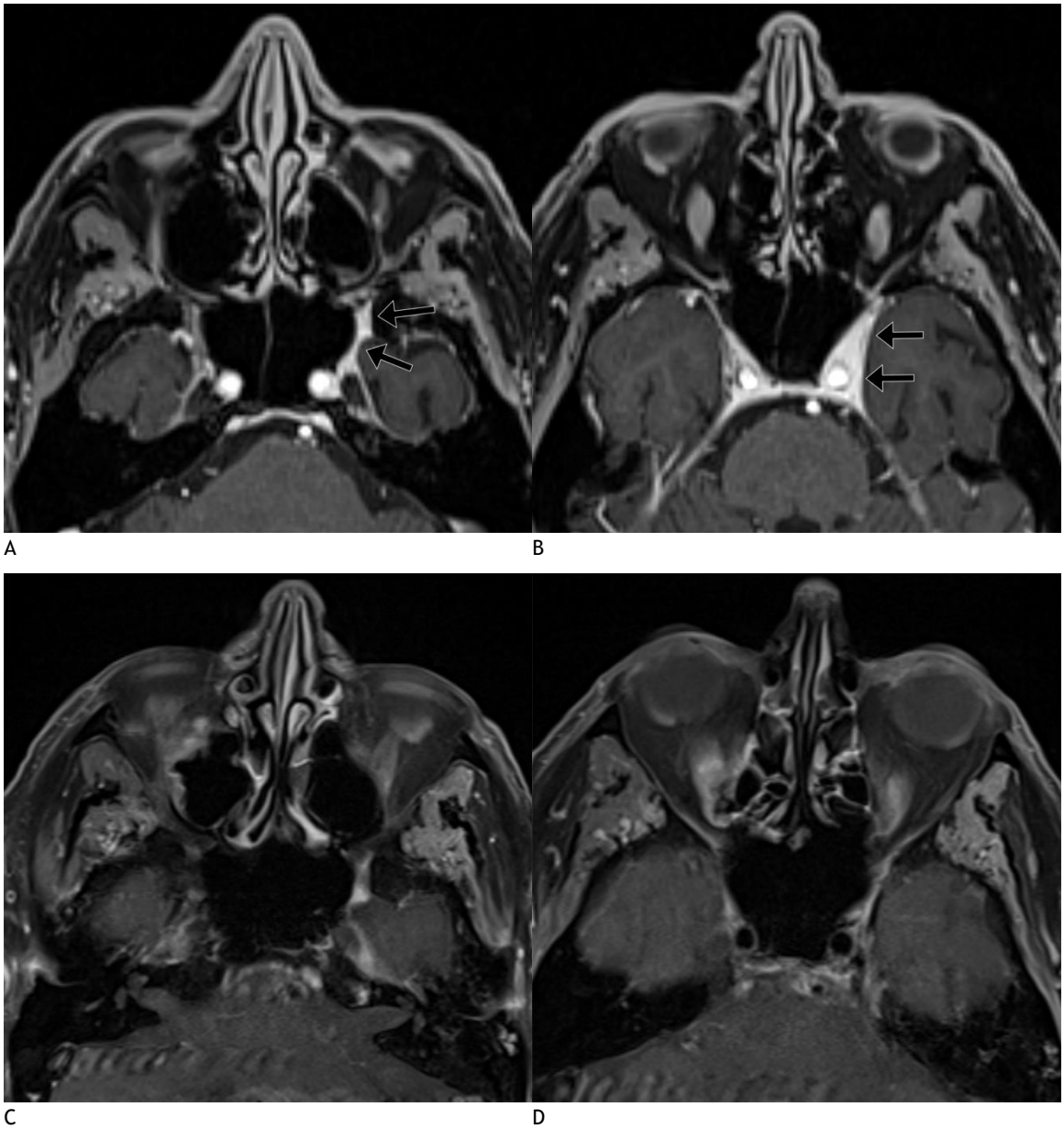

FIG 5. 85-year-old male with spindle cell sarcoma with sinus protocol MRI. T1 VIBE Dixon axial acquisition performed with 0.9mm3 (0.74 mm isotropic) voxels clearly shows tumor (arrows) along (A) left V2 and (B) in the left lateral cavernous sinus wall, neither of which is clearly seen on (C and D) the 2D T1-weighted images with spectral fat suppression with 2mm3 (4x0.7x0.7mm) voxels. The 3D examination shown was performed on a Siemens 3T Prisma Fit system 3 weeks prior to the 2D examination, which was performed on a Siemens 3T Vida system, with no intervening treatment.

DISCUSSION

In this clinical report, we show that it is feasible to leverage commercially available 3D T1-weighted MRI pulse sequence protocols to substantially reduce scan time for clinical face and neck MRI examinations while preserving overall spatial resolution and perhaps improving diagnostic quality. We also describe our experience optimizing these sequences and provide protocol parameters details so that others can replicate our implementations.

For quality assurance, our neuroradiologists were asked by group email and in division staff meetings to send negative, positive, and constructive feedback on the diagnostic quality of these images throughout and following the protocol optimization process via our department's critical results, peer review, and quality assurance closed-loop communication tool (10). We also welcomed and encouraged informal feedback. All feedback requests were open ended. The group initially provided primarily informal mixed feedback on the quality and appropriateness of the 3D acquisition images. The feedback was always preference-based; we identified no cases where diagnostic information was obtained on the 2D images but not the 3D images (although we did identify the converse, as shown in Figures 3, 4, and 6). In addition, we initially ran the 3D protocols alongside the 2D protocols. At that time we were working with the 3D GRE T1-weighted sequence. We gradually phased out the 2D acquisition images on one of our scanners and then on several additional scanners. We did not introduce the 3D TSE T1-weighted protocol until after the 2D protocols were phased out and thus we do not have any same-patient same-examination comparisons of 3D TSE T1-weighted images and 2D TSE T1-weighted images for quantitative SNR and CNR comparisons.

Since our neuroradiologists have become accustomed to the qualitative appearance of the 3D protocol images, we have had no further negative feedback.

The primary technical frustration we have encountered is that, while 3D protocols can be set to automatically generate multi-planar reformats at the scanner on Siemens systems, this reformatting mechanism only reformats the in-phase VIBE Dixon images and cannot be modified to select the fat suppression images for automatic reformatting. We therefore rely on a combination of manual reformatting by the technologists at the scanner and on-the-fly reformatting by the radiologists when reviewing images in our PACS system, which has an excellent 3D multi-planar reformatting tool.

On the positive side, not only can shortening acquisition times help reduce motion artifact, lessen concern for claustrophobia, and increase throughput, it can also provide time to add other useful sequences. In our case, given increasing evidence for DWI utility in head and neck imaging (11,12), we have been able to add DWI back to our face and neck MRI protocols. Time constraints, a focus on high resolution morphologic imaging, and poor-quality DWI images led to removal of DWI from our protocols several years ago. We are also excited to test quantitative arterial spin labeling and dynamic contrast enhancement perfusion imaging (13–16), both of which show considerable promise for diagnostic utility but add acquisition time. Also exciting, but currently investigative, is the potential for 3D synthetic MRI techniques, such as multi-planar multi echo imaging (17,18), that allow acquisition of all contrasts simultaneously and that could allow mathematical derivation and generation of novel contrasts tailored to face and neck applications.

We report only on T1-weighted imaging protocols because we have not successfully implemented 3D T2 techniques with fat suppression. We have attempted to image with 3D T2 STIR techniques, but the fat suppression consistently fails in the region of the nape of the neck. We hypothesize this failure is related to the one-fourth of slice thickness we tried to achieve and the signal decrease due to the much longer echo train length (ETL) for 3D (attempted ETL=150 to keep scan time within 6 minutes) than 2D STIR (ETL = 31), despite our efforts to set similar effective TE for both 3D and 2D STIR. Furthermore, due to the extended ETL in 3D, the acquired echoes can contain signals from recovered fat, resulting in inadequate fat suppression. Vendor product 3D T2-weighted protocols with Dixon-type fat suppression are not currently available.

We may be able to further reduce acquisition times as we explore deep learning reconstruction capabilities on commercially available vendor upgrades. Optimization of 3D T2-weighted imaging with some form of fat suppression would help further reduce scan times and provide 3 plane T2-weighted images for easy cross-referencing. It may also be worth exploring T1-weighted UTE sequences given the ability to visualize bone and cranial nerves on these images (6,19). For now, the optimized commercially available 3D T1-weighted protocols have substantially improved our clinical face and neck MRI examination workflows and also anecdotally appear to have had a positive impact on our diagnostic capabilities.

In summary, our experience shows that it is feasible to leverage commercially available 3D T1-weighted MRI pulse sequence protocols to substantially reduce scan time for clinical face and neck MRI examinations while preserving overall spatial resolution and perhaps improving diagnostic quality.

Table 1: Gradient Time Savings from MRI Protocols on 3T Siemens Prisma and 1.5T Siemens Aera systems for reference

Protocol	2D T1 Version	3D T1 Version	Time Savings	Savings %
3T General	23:05	16:42	6:23	27.7%
3T Nasopharynx	23:42	13:38	10:04	42.5%
3T Oropharynx	26:37	16:33	10:04	37.8%
3T Sinus	24:00	10:42	13:18	55.4%
Mean	*24:21*	*14:24*	*9:57*	*40.9%*
-				
1.5T General	23:15	18:12	5:03	21.7%
1.5T Nasopharynx	24:11	15:26	8:45	36.2%
1.5T Oropharynx	27:33	18:48	8:45	31.8%
1.5T Sinus	23:14	9:28	13:46	59.3%
Mean	*24:33*	*15:29*	*9:05*	*37.0%*

ACKNOWLEDGMENTS

The authors have no acknowledgments.

Disclosure forms provided by the authors are available with the full text and PDF of this article at www.ajnr.org.

REFERENCES

1. Razek AAKA, King A. MRI and CT of Nasopharyngeal Carcinoma. American Journal of Roentgenology. 2012 Jan 1;198(1):11–8.
2. Chong VFH, Fan YF. Skull base erosion in nasopharyngeal carcinoma: Detection by CT and MRI. Clinical Radiology. 1996 Sep 1;51(9):625–31.
3. Moonis G, Cunnane MB, Emerick K, Curtin H. Patterns of Perineural Tumor Spread in Head and Neck Cancer. Magnetic Resonance Imaging Clinics. 2012 Aug 1;20(3):435–46.
4. Cho SJ, Lee JH, Suh CH, Kim JY, Kim D, Lee JB, et al. Comparison of diagnostic performance between CT and MRI for detection of cartilage invasion for primary tumor staging in patients with laryngo-hypopharyngeal cancer: a systematic review and meta-analysis. Eur Radiol. 2020 Jul 1;30(7):3803–12.
5. Guenette JP, Ben-Shlomo N, Jayender J, Seethamraju RT, Kimbrell V, Tran NA, et al. MR Imaging of the Extracranial Facial Nerve with the CISS Sequence. AJNR Am J Neuroradiol. 2019 Nov;40(11):1954–9.
6. Guenette JP, Seethamraju RT, Jayender J, Corrales CE, Lee TC. MR Imaging of the Facial Nerve through the Temporal Bone at 3T with a Noncontrast Ultrashort Echo Time Sequence. AJNR Am J Neuroradiol. 2018 Oct;39(10):1903–6.
7. Casselman JW, Kuhweide R, Deimling M, Ampe W, Dehaene I, Meeus L. Constructive interference in steady state-3DFT MR imaging of the inner ear and cerebellopontine angle. AJNR Am J Neuroradiol. 1993 Feb;14(1):47–57.
8. Alkan A, Sigirci A, Ozveren MF, Kutlu R, Altinok T, Onal C, et al. The cisternal segment of the abducens nerve in man: three-dimensional MR imaging. Eur J Radiol. 2004 Sep;51(3):218–22.
9. Dixon WT. Simple proton spectroscopic imaging. Radiology. 1984 Oct;153(1):189–94.
10. Glazer DI, Zhao AH, Lacson R, Burk KS, DiPiro PJ, Kapoor N, et al. Use of a PACS Embedded System for Communicating Radiologist to Technologist Learning Opportunities and Patient Callbacks. Curr Probl Diagn Radiol. 2022;51(4):511–6.
11. Miracle AC, El-Sayed IH, Glastonbury CM. Diffusion weighted imaging of esthesioneuroblastoma: Differentiation from other sinonasal masses. Head Neck. 2019 May;41(5):1161–4.
12. Yeom KW, Lober RM, Mobley BC, Harsh G, Vogel H, Allagio R, et al. Diffusion-Weighted MRI: Distinction of Skull Base Chordoma from Chondrosarcoma. Am J Neuroradiol. 2013 May;34(5):1056–61.
13. Amukotuwa SA, Marks MP, Zaharchuk G, Calamante F, Bammer R, Fischbein N. Arterial Spin-Labeling Improves Detection of Intracranial Dural Arteriovenous Fistulas with MRI. AJNR Am J Neuroradiol. 2018 Apr;39(4):669–77.
14. Sun Z, Hu S, Ge Y, Jin L, Huang J, Dou W. Can Arterial Spin Labeling Perfusion Imaging be Used to Differentiate Nasopharyngeal Carcinoma From Nasopharyngeal Lymphoma? J Magn Reson Imaging. 2021 Apr;53(4):1140–8.
15. Baba A, Kurokawa R, Rawie E, Kurokawa M, Ota Y, Srinivasan A. Normalized Parameters of Dynamic Contrast-Enhanced Perfusion MRI and DWI-ADC for Differentiation between Posttreatment Changes and Recurrence in Head and Neck Cancer. AJNR Am J Neuroradiol. 2022 Aug;43(8):1184–9.
16. Ota Y, Liao E, Capizzano AA, Kurokawa R, Bapuraj JR, Syed F, et al. Diagnostic Role of Diffusion-Weighted and Dynamic Contrast-Enhanced Perfusion MR Imaging in Paragangliomas and Schwannomas in the Head and Neck. AJNR Am J Neuroradiol. 2021 Oct;42(10):1839–46.
17. Cheng CC, Preiswerk F, Hoge WS, Kuo TH, Madore B. Multipathway multi-echo (MPME) imaging: all main MR parameters mapped based on a single 3D scan. Magn Reson Med. 2019;81(3):1699–713.
18. Cheng CC, Preiswerk F, Madore B. Multi-pathway multi-echo acquisition and neural contrast translation to generate a variety of quantitative and qualitative image contrasts. Magn Reson Med. 2020 Jun;83(6):2310–21.
19. Bracher AK, Hofmann C, Bornstedt A, Hell E, Janke F, Ulrici J, et al. Ultrashort echo time (UTE) MRI for the assessment of caries lesions. Dentomaxillofacial Radiology. 2013 Apr 24;42(6):20120321.

SUPPLEMENTAL FILES

2D TSE T1-weighted Reference Protocols

To allow high spatial resolution within reasonable examination times, face and neck MRI examinations are ideally focused on a target region. T1-weighted turbo spin echo sequences have excellent soft tissue contrasts for face and neck imaging given that neoplasms are typically fat replacing or fat displacing. This sequence is therefore the mainstay of our protocols. For our traditional 2D T1-weighted sequences, the protocol is configured for 3 mm slice thickness, no gap, and 0.5 mm in plane resolution. We run this sequence in the axial plane and we generally also include this sequence in the coronal plane, especially in protocols where the oral cavity, skull base neural foramina, or paranasal sinuses require close evaluation. We run a lower resolution T1-weighted turbo spin echo sequence in the sagittal plane. These sequences provide us with 3 planes of T1-weighted imaging through the region of interest. In addition, we run a T2 STIR from the mid orbits to manubrium to assess the full neck for adenopathy while also providing fluid-sensitive information for the area of primary interest.

For indications where the concerns are less focal and more on characterizing or discerning the extent of gross soft tissue abnormalities (e.g. trans-spatial venolymphatic malformations or infiltrating carcinomas, sarcomas of the mid/lower neck, and new palpable masses of the mid/lower neck), we have a protocol in which we obtain somewhat thicker axial and coronal T1-weighted images with 4 mm slice thickness, no gap, covering the entire neck from the mid orbits to manubrium.

Given the susceptibility effects of fat suppression techniques at air-tissue interfaces and how these effects can obscure or distort the cavernous sinuses and neural foramina at the skull base, we favor T1-weighted images without fat suppression for our higher resolution region-specific protocols. However, given the variable preferences within our group and our radiation oncologists' preference for fat suppression images, we also run a lower resolution post-contrast T1-weighted turbo spin echo sequence with spectral fat suppression. For the lower resolution non-focal protocol we run the post-contrast axial and coronal T1-weighted sequences with fat suppression.

Scan ranges with a list of pulse sequences for each of our protocols are outlined in our publicly available protocol guide (1). Protocol parameters are listed in Supplemental Table 2. There are some parameter differences across these protocols due to modifications made ad hoc by technologists over time. Anecdotally, we have found that only minor adjustments are typically needed to translate these protocols across Siemens and GE systems. We have implemented these protocols on Siemens 3T Vida, 3T Prisma, and 3T PrismaFit systems running platforms VE11C and XA30 and on a GE 3T Premier system running MR30. We have also implemented the protocols on a Siemens 1.5T Aera running VE11C. On Siemens scanners we typically utilize the Siemens 20-channel head and neck coil with occasional use of a Siemens 64-channel head and neck coil, which we have available only on a few scanners. On our GE scanner we use a GE 21-channel AIR coil. We do not have first-hand experience translating these protocols to other vendor platforms.

References

1. Guenette J. Head and Neck MRI Protocols. https://doi.org/10.7910/DVN/KEXYZL.

Supplemental Table 2: 3D T1-Weighted Sequence Protocols for Face and Neck MRI from 3T Siemens Prisma and 1.5T Siemens Aera Systems on VE11C for Reference

Field Strength	Acquisition Type	Acquisition Plane	Contrast	Fat Suppression	Phase Encoding	Voxel Dimensions	Slices	FOV (mm)	TR (ms)	TE1 (ms)	TE2 (ms)	NEX	Flip Angle	Acceleration Mode	Acceleration Factor PE	Acceleration Factor 3D	Scan Time	Protocols
3T	TSE	Sagittal	Pre	Off	A>>P	1.0x1.0x1.0	176	256	600	19	NA	1.4	variable	CAIPIRINHA	2	2	4:51	General
3T	TSE	Axial	Pre	Off	R>>L	0.9x0.9x0.8	144	240	600	20	NA	1.8	variable	GRAPPA	3	1	5:28	Nasopharynx, Oropharynx
1.5T	TSE	Sagittal	Pre	Off	A>>P	1.0x1.0x1.0	160	256	500	17	NA	2	variable	GRAPPA	1	2	5:31	General
1.5T	TSE	Axial	Pre	Off	R>>L	0.9x0.9x0.9	144	240	500	18	NA	2	variable	GRAPPA	1	2	5:45	Nasopharynx, Oropharynx
3T	GRE	Sagittal	Post	Dixon	A>>P	1.0x1.0x1.0	176	256	5.9	2.46	3.69	2	9	GRAPPA	3	1	4:35	General
3T	GRE	Axial	Post	Dixon	R>>L	0.9x0.9x0.9	128	240	5.6	2.46	3.69	1	9	None	None	None	3:49	Nasopharynx, Oropharynx
3T	GRE	Coronal	Pre	None	R>>L	1.0x1.0x1.0	128	200	5.53	2.28	NA	1	9	None	None	None	2:32	Sinus
3T	GRE	Coronal	Post	Dixon	R>>L	1.0x1.0x1.0	128	200	6.29	2.46	3.69	1	9	None	None	None	3:01	Sinus
1.5T	GRE	Sagittal	Post	Dixon	A>>P	1.0x1.0x1.0	160	256	7.03	2.39	4.77	2	10	GRAPPA	1	2	5:36	General
1.5T	GRE	Axial	Post	Dixon	R>>L	0.9x0.9x0.9	144	240	7.76	2.39	4.77	1	9	None	None	None	5:13	Nasopharynx, Oropharynx
1.5T	GRE	Coronal	Pre	None	R>>L	1.0x1.0x1.0	128	200	5.42	2.48	NA	1	9	None	None	None	2:46	Sinus
1.5T	GRE	Coronal	Post	Dixon	R>>L	1.0x1.0x1.0	128	200	7.63	2.39	4.77	1	9	None	None	None	3:42	Sinus

Supplemental Table 2: 2D TSE T1-Weighted Sequence Protocol Parameters for Face and Neck MRI

3T MRI Protocols from a Siemens Prisma system running VE11C for reference

Acquisition Plane	Contrast	Fat Suppression	Phase Encoding	Voxel Dimensions	Voxel Volume (mm^3)	Slices	FOV (mm)	TR (ms)	TE (ms)	NEX	Concat-enations	Flip Angle	Acceleration Mode	Acceleration Factor	Scan Time	Protocols
Sagittal	Pre	Off	A>>P	3.0x0.8x0.8	1.92	30	210	495	8.6	2	2	150	GRAPPA	2	1:57	General
Axial	Pre	Off	A>>P	4.0x0.4x0.4	0.64	60	200	786	9.6	2	2	150	GRAPPA	2	3:49	General
Axial	Post	Strong	A>>P	4.0x0.4x0.4	0.64	60	200	814	9.6	2	3	150	GRAPPA	2	5:56	General
Coronal	Post	Strong	R>>L	4.0x0.8x0.8	2.56	30	240	700	8.7	2	2	150	GRAPPA	2	4:07	General
Axial	Pre/Post	Off	R>>L	3.0x0.5x0.5	0.75	40	170	556	9.2	1	3	130	None	None	3:35	Nasopharynx, Oropharynx
Coronal	Pre/Post	Off	R>>L	3.0x0.5x0.5	0.75	40	170	628	9.4	1	2	120	None	None	3:41	Nasopharynx, Oropharynx
Axial	Post	Strong	R>>L	4.0x0.6x0.6	1.44	30	160	826	9.4	1	2	130	None	None	2:52	Nasopharynx, Oropharynx
Coronal	Pre/Post	Off	R>>L	3.0x0.5x0.5	0.75	40	160	612	9.4	1	3	120	None	None	3:57	Sinus
Axial	Pre/Post	Off	R>>L	3.0x0.3x0.3	0.27	40	160	650	8.6	2	2	123	None	None	4:07	Sinus
Axial	Post	Strong	R>>L	3.0x0.6x0.6	1.08	40	160	671	13	1	4	130	None	None	4:16	Sinus

1.5T MRI Protocols from a Siemens Aera system running VE11C for reference

Acquisition Plane	Contrast	Fat Suppression	Phase Encoding	Voxel Dimensions	Voxel Volume (mm^3)	Slices	FOV (mm)	TR (ms)	TE (ms)	NEX	Concat-enations	Flip Angle	Acceleration Mode	Acceleration Factor	Scan Time	Protocols
Sagittal	Pre	Off	A>>P	3.0x0.9x0.9	2.43	30	220	495	8.1	2	2	150	GRAPPA	2	2:09	General
Axial	Pre	Off	A>>P	4.0x0.4x0.4	0.64	52	220	752	11	2	2	150	GRAPPA	2	3:40	General
Axial	Post	Strong	A>>P	4.0x0.4x0.4	0.64	52	220	700	11	1	4	150	GRAPPA	2	3:46	General
Coronal	Post	Strong	R>>L	4.0x0.8x0.8	2.56	40	240	750	8.7	2	3	150	GRAPPA	2	6:35	General
Axial	Pre/Post	Off	R>>L	3.0x0.6x0.6	1.08	40	180	556	7.5	1	3	130	None	None	3:35	Nasopharynx, Oropharynx
Coronal	Pre/Post	Off	R>>L	3.0x0.5x0.5	0.75	40	170	632	9.7	1	2	120	None	None	4:03	Nasopharynx, Oropharynx
Axial	Post	Strong	R>>L	4.0x0.7x0.7	1.96	30	180	826	7.2	1	2	130	None	None	2:52	Nasopharynx, Oropharynx
Coronal	Pre/Post	Off	R>>L	3.0x0.6x0.6	1.08	40	180	469	8.8	1	3	120	None	None	2:40	Sinus
Axial	Pre/Post	Off	R>>L	3.0x0.4x0.4	0.48	40	180	706	9.3	2	2	123	None	None	4:28	Sinus
Axial	Post	Strong	R>>L	3.0x0.7x0.7	1.47	40	180	671	11	1	4	130	None	None	4:16	Sinus